# Frequency-domain Analysis for Infinite Resets Systems*

Zhang, Xinxin; Hosseinnia, S. Hassan

**DOI**
10.1109/ICM54990.2023.10101919

**Publication date**
2023

**Document Version**
Final published version

**Published in**
Proceedings - 2023 IEEE International Conference on Mechatronics, ICM 2023

# Frequency-domain Analysis for Infinite Resets Systems*

Xinxin Zhang
*dept. Precision and Microsystems Engineering (PME)*
*Delft University of Technology*
Mekelweg 2, Delft, NL
X.Zhang-15@tudelft.nl (0000-0003-4656-3338)

S. Hassan HosseinNia*
*dept. Precision and Microsystems Engineering (PME)*
*Delft University of Technology*
Mekelweg 2, Delft, NL
S.H.HosseinNiaKani@tudelft.nl (0000-0002-7475-4628)

2023 IEEE International Conference on Mechatronics (ICM) | 978-1-6654-6661-5/23/$31.00 ©2023 IEEE | DOI: 10.1109/ICM54990.2023.10101919

***Abstract*—Reset control systems have possessed the potential to meet the demands of machines, such as faster response times, improved disturbance rejection and enhanced tracking performance. However, prior research on the analysis and design of reset controllers has been restricted to the assumption of two resets per period, neglecting multiple-reset scenarios. In light of this, we focus on the frequency-domain analysis of Infinite-reset Control Systems, which serve as the limit case of multiple-reset control systems, and propose a new model for their analysis. Through this model, the sensitivity functions of Infinite-reset Control Systems are characterised, linking their frequency-domain and time-domain behaviour. The effectiveness of the infinite-reset system is evaluated through simulation of a reset control system case. The results reveal that the infinite-reset system demonstrates improved accuracy in prediction in multiple-reset systems compared to the previous analysis methods. Furthermore, this study provides a deeper understanding of the reset systems.**

***Index Terms*—reset control system, infinite-reset systems, frequency-domain analysis, sensitivity functions**

## I. Introduction

The use of controllers in the precision motion industry is crucial for achieving precise positioning in machines. However, it can be challenging for traditional linear compensators to meet the demands for high speed and precision due to the limitations imposed by the Bode gain-phase relationship and the waterbed effect [1]. As a result, the development of nonlinear controllers that can overcome these limitations is necessary. One such potential alternative is the reset controller (RC), which has the advantage of being easily integrated into conventional design frameworks and has thus been gaining increasing attention in both academic and industrial settings [2], [3].

The concept of the Reset Controller (RC) was first introduced by Clegg in 1958 with the development of the Clegg Integrator (CI) [4]. The CI, a linear integrator with an internal reset mechanism, has the ability to reset its output to zero when the input signal crosses zero. Through the use of Describing Function (DF) analysis, it was found that the CI has a phase lag of only 38.1° compared to the 90° phase lag of a traditional linear integrator. This phase advantage of the CI demonstrates its ability to overcome the Bode gain-phase trade-off restriction. In the 1970s, Horowitz, et al. developed the first-order reset element (FORE) and a quantitative design procedure for it [5], [6]. The FORE, which combines a first-order linear low-pass filter with a reset law, has been found to perform well in disturbance-tolerance. Subsequently, the field of RC has attracted increasing attention, leading to the development of various reset elements, see [7], [8], [9], [10], [11], [12], [13].

Frequency-domain techniques are easy-to-use, 'industry-friendly' design tools for reset control systems (RCSs) [14]. In open-loop, Higher-order sinusoidal input describing function (HOSIDF) have been utilised to analyse the frequency-domain properties of each harmonic of RCSs [15], [16] [17]. In closed-loop, numerical evaluation for RCSs was proposed in [18], however, this method is not suitable for the loop-shaping technique. In [3], the authors developed a frequency-domain based analysis method for RCSs in closed-loop but failed to include reset actions of higher harmonics in output signals, which will cause deviations. In [19], a model for analysing closed-loop RCSs was developed to overcome these deviations and achieve precise loop-shaping analysis of Single-input single-output (SISO) RCSs.

However, the above analytical methods for RCSs in closed-loop are limited to scenarios with two resets per period, thereby excluding multiple-reset situations, such as in [20], [21]. The frequency-domain characteristics of Multiple-reset Control Systems (MRCSs) are not well-understood. However, directly analysing the nonlinear elements of MRCSs is redundant. Therefore, we investigates the frequency-domain properties of the extreme case of the MRCS: Infinite-reset Control System (IRCS).

The overall structure of the study takes the form of five sections. Section II introduces the definition of the RCS, its stability and convergence analysis, and analysis methods for RCSs. Section III demonstrates the two main contributions of this study: (1) We demonstrate that all closed-loop RCSs can be separated into their base-linear systems (BLSs) and corresponding nonlinear components; and (2) we develop a new frequency-domain based model for analysing the IRCSs. Additionally, sensitivity functions of the IRCS that connect the frequency-domain and the time-domain are developed. Then, the performance of the proposed technique is validated by the

*Coppresponding author: S. Hassan HosseinNia.

simulation in an RCS in section IV, showing its effectiveness. Finally, concluding remarks are illustrated in section V. It should be notes that the IRCS is an extreme case. In practice, RCSs will not experience infinite reset intervals and lead to Zenoness.

## II. Preliminaries

This section presents the definition, the stability and convergence conditions, and current frequency-domain analysis tools for the RCS.

### A. General Reset Control System

Figure 1 shows the block diagram of a general RCS in closed-loop. It includes a reset controller represented by the block $\mathcal{C}$, a plant embodied by the block $\mathcal{P}$, in which $r(t)$, $e(t)$, $u(t)$, and $y(t)$ are the reference input signal, error, control input, and system output signals respectively. In this study, we have restricted our attention to the analysis of SISO RCSs with the reference input signal given by $r(t)$, and the process disturbance $d(t)$ and measurement noise $n(t)$ are not taken into consideration.

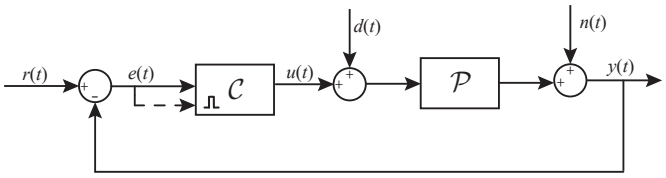


Fig. 1: Block diagram of the RCS, where the dashed-line represents the resetting action.

The RCS is a class of hybrid systems whose flow map is identical to its linear counterpart, while the jump map is a resetting mechanism [22], [23]. The jump set is based on different reset laws. The classical reset law is "zero-crossing law" where the output will be reset when the input signal crosses zero. The state-space model of a general RCS can be represented as follows:

$$\mathcal{C} = \begin{cases} \dot{x}_r(t) = A_R x_r(t) + B_R e(t), & \text{when } e(t) \neq 0 \\ x_r(t^+) = A_\rho x_r(t), & \text{when } e(t) = 0 \\ u(t) = C_R x_r(t) + D_R e(t), \end{cases} \tag{1}$$

where $x_r(t) \in \mathbb{R}^{n_c}$ is the RC state, and $n_c$ is the number of the states; $A_R$, $B_R$, $C_R$, $D_R$ together describe the dynamic of the BLS; $A_\rho$ defines the reset matrix:

$$A_\rho = \begin{bmatrix} \gamma & \\ & I_l \end{bmatrix}, \gamma = \text{diag}(\gamma_1, \gamma_2, \cdots, \gamma_r), \tag{2}$$

with $\gamma_r \in [-1, 1]$ showing that the RC state resets to its proportional value. There are two type of states in $A_\rho$: nonlinear reset states with number of $r$ , and $l$ linear states, where $n_c = r + l$.

In Fig. 1, the state-space representations of the plant $\mathcal{P}$ are defined as

$$\mathcal{P} = \begin{cases} \dot{x}_p(t) = A_P x_p(t) + B_P u(t), \\ y(t) = C_P x_p(t), \end{cases} \tag{3}$$

where $A_P$, $B_P$, $C_P$ describe the dynamic of the plant, $x_p \in \mathbb{R}^{n_p}$ is the plant state, and $n_p$ is the number of plant states.

Neglecting the exogenous input signal $r(t)$ and combining $\mathcal{C}$ in (1) and $\mathcal{P}$ in (3), the state-space representatives of the closed0loop RCS denoted by $\mathcal{H}$ is given as

$$\mathcal{H} = \begin{cases} \dot{x}(t) = A_{cl} x(t), & \text{when } x \notin J \\ x(t^+) = A_r x(t), & \text{when } x \in J \\ y(t) = C_{cl} x(t), \end{cases} \tag{4}$$

where $x^T = [{x_r}^T \ {x_p}^T] \in \mathbb{R}^{n_h}$ with $n_h = n_c + n_p$ being the number of $\mathcal{H}$ states, and $J := \{x \in \mathbb{R}^{n_h} | C_{cl} x = 0\}$ is the set of reset instants meeting the condition of $e(t) = 0$. The state-space matrices are given as

$$A_{cl} = \begin{bmatrix} A_R & -B_R C_P \\ B_P C_R & A_P \end{bmatrix}, C_{cl} = \begin{bmatrix} 0 & C_P \end{bmatrix}, A_r = \begin{bmatrix} A_\rho & \\ & I \end{bmatrix}. \tag{5}$$

### B. The Stability and Convergence Conditions for RCSs

For an RCS, we need to guarantee its stability and convergence. The $H_\beta$ condition presented in proposition 1 provides sufficient conditions for $\mathcal{L}_\infty$ (bounded input bounded state) stability for the closed-loop RCS driven by periodic inputs.

**Proposition 1.** *($H_\beta$ condition [7], [24]) The RCS in (4) is quadratically stable if and only if the $H_\beta$ condition holds, i.e., there exists a $\beta \in \mathbb{R}^r$ and a positive definite matrix $P_r \in \mathbb{R}^{r \times r}$ such that the transfer function*

$$H_\beta(s) \triangleq \begin{bmatrix} \beta C_p & 0_{r \times l} & P_r \end{bmatrix} (sI - A_{cl})^{-1} \begin{bmatrix} 0 \\ 0_{r \times l}^T \\ I_{r \times r} \end{bmatrix}, \tag{6}$$

*is Strictly Positive Real (SPR) and additionally a non-zero reset matrix $A_\rho$ satisfies the condition*

$$A_\rho^T P_r A_\rho - P_r \leqslant 0. \tag{7}$$

If the $H_\beta$ condition holds, then RCS has the uniform bounded-input bounded state (UBIBS) property. Besides, [25] provides the $\mathcal{L}_2$ stability of reset systems. Except for the stability conditions, for nonlinear systems, extra convergence conditions for the closed-loop RCS under periodic inputs are provided in [26], [27].

### C. Frequency-domain Analysis Tool for Two-reset Control System

In open-loop, HOSIDF is applied to analyse RCSs [28]. The function $H_n(\omega)$ is defined to describe the ratio of the control input signal $u(t)$ to the error signal $e(t)$ at steady-states, where $n$ is the number of harmonics and $\omega$ is the frequency of input signal $e(t)$. $H_n(\omega)$ [3], [28] is given by

$$H_n(\omega) = \begin{cases} C_R(j\omega I - A_R)^{-1}(I + j\Theta_D(\omega))B_R + D_R, & \text{for } n = 1 \\ C_R(jn\omega I - A_R)^{-1} j\Theta_D(\omega) B_R, & \text{for odd } n \geqslant 2 \\ 0, & \text{for even } n \geqslant 2 \end{cases} \tag{8}$$

with

$$\begin{aligned}\Lambda(\omega) &= \omega^2 I + {A_R}^2,\\ \Delta(\omega) &= I + e^{(\frac{\pi}{\omega}A_R)},\\ \Delta_r(\omega) &= I + A_\rho e^{(\frac{\pi}{\omega}A_R)},\\ \Gamma_r(\omega) &= \Delta_r^{-1}(\omega)A_\rho\Delta(\omega)\Lambda^{-1}(\omega),\\ \Theta_D(\omega) &= \frac{-2\omega^2}{\pi}\Delta(\omega)[\Gamma_r(\omega) - \Lambda^{-1}(\omega)].\end{aligned} \tag{9}$$

In closed-loop, assuming there are two reset instants per period, the sensitivity functions of a RCS are given in the following Proposition [19].

**Proposition 2.** *(Sensitivity functions for the RCS with two reset instants in closed-loop) In a RCS (4), for a sinusoidal reference signal $r(t) = \sin(\omega t)$, $\mathcal{S}_n(\omega)$ $(n \in \mathbb{N})$ and $\mathcal{T}_n(\omega)$ are defined to be the n-th sensitivity function and complementary sensitivity function of the RCS in closed-loop given by*

$$\mathcal{S}_n(\omega) = \begin{cases} \frac{1}{1+\mathcal{L}_O(\omega)}, & \text{for } n = 1\\ -\frac{\Gamma\mathcal{L}_{NL}(n\omega)}{1+\mathcal{L}(n\omega)} \cdot \frac{e^{-jn\angle\mathcal{L}_O(\omega)}}{|1+\mathcal{L}_O(n\omega)|}, & \text{for odd } n \geqslant 2\\ 0, & \text{for even } n \geqslant 2 \end{cases} \tag{10}$$

$$\mathcal{T}_n(\omega) = \begin{cases} \frac{\mathcal{L}_O(\omega)}{1+\mathcal{L}_O(\omega)}, & \text{for } n = 1\\ \frac{\Gamma\mathcal{L}_{NL}(n\omega)}{1+\mathcal{L}(n\omega)} \cdot \frac{e^{-jn\angle\mathcal{L}_O(\omega)}}{|1+\mathcal{L}_O(n\omega)|}, & \text{for odd } n \geqslant 2\\ 0, & \text{for even } n \geqslant 2 \end{cases} \tag{11}$$

*with*

$$\begin{aligned}\mathcal{L}_O(n\omega) &= \mathcal{L}(n\omega) + \Gamma\mathcal{L}_{NL}(n\omega),\\ \mathcal{L}(n\omega) &= R_L(n\omega)\mathcal{P}(\omega),\\ \mathcal{L}_{NL}(n\omega) &= R_{NL}(n\omega)\mathcal{P}(n\omega),\\ R_L(\omega) &= C_R(j\omega I - A_R)^{-1}B_R + D_R,\\ R_{NL}(n\omega) &= \frac{1}{n}R_\delta(n\omega)R_\delta^{-1}(\omega)\left[H_1(\omega) - R_L(\omega)\right],\end{aligned} \tag{12}$$

*where $\Gamma(\omega)$ is given by*

$$\begin{aligned}\Gamma(\omega) &= 1/\left(1 - \frac{\sum_{n=3}^{\infty}\zeta(n\omega)\eta(n\omega)}{\eta(\omega)}\right),\\ \zeta(n\omega) &= \frac{-|\mathcal{L}_{nl}(n\omega)|\cos(\angle\mathcal{L}_{nl}(n\omega))}{1 + |\mathcal{L}_{bl}(n\omega)|\cos(\angle\mathcal{L}_{bl}(n\omega))},\\ \eta(n\omega) &= (A_\rho - I)|C_{bl}(\omega)|\sin(r\pi + \angle C_{bl}(\omega)),\ (r \in \mathbb{N}).\end{aligned} \tag{13}$$

However, there is a lack of frequency-domain analysis methods for multiple-reset control systems. To address this gap, we develop a frequency-domain analysis method for multiple-reset systems based on the limit-case of infinite-reset systems.

## III. Methodology

This section is primarily focused on the development of a frequency-domain analysis method for Infinite-reset Control Systems (IRCSs). Additionally, a comparison metric is established to evaluate the performance of the proposed method compared to previous methods. Note that IRCSs are are limit cases of MRCSs and are distinct from the zenoness scenario.

### A. The Piece-wise Model of RCSs

In this subsection, we show the outputs of a general RCS are piece-wise functions. Furthermore, RCSs are proved to be the sum of their BLSs and stair-step inputs.

Suppose that the reference signal $r(t)$ in Fig. 1 is a sinusoidal wave given by $r(t) = R_0\sin(\omega t)$ and $\mathcal{C}_{bl}(\omega)$ is the base-linear controller. The open-loop transfer function, sensitivity function, complementary sensitivity function, and control sensitivity function of the BLS denoted by $\mathcal{L}_{bl}(\omega)$, $\mathcal{S}_{bl}(\omega)$, $\mathcal{T}_{bl}(\omega)$, and $\mathcal{CS}_{bl}(\omega)$ respectively are given by

$$\begin{aligned}\mathcal{L}_{bl}(\omega) &= \mathcal{C}_{bl}(\omega)\mathcal{P}(\omega),\\ \mathcal{S}_{bl}(\omega) &= \frac{1}{1+\mathcal{L}_{bl}(\omega)},\\ \mathcal{T}_{bl}(\omega) &= \frac{\mathcal{L}_{bl}(\omega)}{1+\mathcal{L}_{bl}(\omega)},\\ \mathcal{CS}_{bl}(\omega) &= \frac{\mathcal{C}_{bl}(\omega)}{1+\mathcal{L}_{bl}(\omega)}.\end{aligned} \tag{14}$$

The control input signal $u_{bl}(t)$, error signal $e_{bl}(t)$ and output signal $y_{bl}(t)$ of the BLS are given by

$$\begin{aligned}u_{bl}(t) &= R_0\,|\mathcal{CS}_{bl}(\omega)|\sin(\omega t + \angle\mathcal{CS}_{bl}(\omega)),\\ e_{bl}(t) &= R_0\,|\mathcal{S}_{bl}(\omega)|\sin(\omega t + \angle\mathcal{S}_{bl}(\omega)),\\ y_{bl}(t) &= R_0\,|\mathcal{T}_{bl}(\omega)|\sin(\omega t + \angle\mathcal{T}_{bl}(\omega)).\end{aligned} \tag{15}$$

$\mathcal{R}_\delta(\omega)$ is defined for calculation convenience given by

$$\mathcal{R}_\delta(\omega) = C_R(j\omega I - A_R)^{-1}j\omega I. \tag{16}$$

The unit Heaviside step function $h(t)$ is defined by

$$h(t) := \begin{cases} 1, & t > 0\\ 0, & t \leqslant 0 \end{cases} \tag{17}$$

$h_s(t)$ and $h_{ps}(t)$ represent the step responses of $h(t)$ with respect to $\mathcal{R}_\delta(\omega)\mathcal{S}_{bl}(\omega)$ and $\mathcal{R}_\delta(\omega)\mathcal{P}(\omega)\mathcal{S}_{bl}(\omega)$:

$$\begin{aligned}h_s(t) &= \mathscr{F}^{-1}[H(\omega)\cdot\mathcal{R}_\delta(\omega)\mathcal{S}_{bl}(\omega)],\\ h_{ps}(t) &= \mathscr{F}^{-1}[H(\omega)\cdot\mathcal{R}_\delta(\omega)\mathcal{P}(\omega)\mathcal{S}_{bl}(\omega)],\end{aligned} \tag{18}$$

with $H(\omega)$ being the Fourier transform of $h(t)$.

$t_R := \{e(t_i) = 0 | i \in \mathbb{N}\}$ is defined to be the set of reset instants, with $t_0 = 0$. $t_i^-$ denotes the before-reset state while the $t_i^+$ denotes the after-reset state. Afterwards, uppercase letters are used to indicate the frequency-domain components, while lowercases denote time-domain ones as per convention. The RCSs in the paper are under the zero initial condition.

**Lemma 1.** *(The first reset instant) Suppose the input signal of the RCS is a sinusoidal wave given by $r(t) = R_0\sin(\omega t)$, by ignoring the initial transient response, the first reset instant $t_1$ can be approximated as follows:*

$$t_1 = \frac{\pi - \angle(\mathcal{S}_{bl}(\omega))}{\omega}. \tag{19}$$

*Proof.* The first reset instant meets the condition that the base-linear error signal $e_{bl}(t)$ hits to zero for the first time. $e_{bl}(t)$ in steady-state is given by

$$e_{bl}(t) = R_0|\mathcal{S}_{bl}(\omega)|\sin(\omega t + \angle(\mathcal{S}_{bl}(\omega))), \tag{20}$$

so the first solution of $e_{bl}(t_1) = 0$ is the first reset instant $t_1$ of the RCS as given in (19). □

**Lemma 2.** *(The piece-wise formats of RCSs outputs) In a SISO RCS, the input signal is defined as a sinusoidal wave $r(t) = R_0 \sin(\omega t)$, and the number of reset instants in one period is denoted by $\mu$, the control input signal $u(t)$, output signal $y(t)$, and error signal $e(t)$ are piece-wise functions that are defined by the reset instants $t_i \in t_R$. Specifically, for the time interval between two reset instants $(t_i, t_{i+1})$, the piece-wise functions for the control input signal, output signal, and error signal are denoted by $u_{i+1}(t)$, $y_{i+1}(t)$, and $e_{i+1}(t)$, respectively, and are mathematically represented as follows.*

$$\begin{aligned} u_{i+1}(t-t_i) &= u_i(t-t_{i-1}) - (1-\gamma)u_i(t_i^-)\cdot h_s(t-t_i),\\ y_{i+1}(t-t_i) &= y_i(t-t_{i-1}) - (1-\gamma)u_i(t_i^-)\cdot h_{ps}(t-t_i),\\ e_{i+1}(t-t_i) &= e_i(t-t_{i-1}) + (1-\gamma)u_i(t_i^-)\cdot h_{ps}(t-t_i). \end{aligned} \tag{21}$$

*Proof.* At an arbitrary reset instant $t_i \in t_R (i \in \mathbb{N})$, the state $x(t_i)$ of the RC is reset to its proportional value $\gamma x(t_i)$, where $\gamma$ is a constant in the range $[-1, 1]$. The reset action during two arbitrary reset instants $(t_i, t_{i+1})$ is equivalent to introducing a step signal with amplitude $(\gamma - 1)u_i(t_i^-)$ as a disturbance in the state $x(t)$. Therefore, the piece-wise functions for $u_{i+1}(t)$, $y_{i+1}(t)$, and $e_{i+1}(t)$ can be derived as shown in (21). □

**Theorem 1.** *(The time-domain model for a general RCS) In a SISO RCS, the input signal $r(t)$ is defined as $r(t) = R_0 \sin(\omega t)$, and the number of reset instants in one period is given by $\mu$. The output $y(t)$ is divided in two signals: its base-linear output $y_{bl}(t)$, and a nonlinear output denoted by $y_{nl}(t)$ as shown below.*

$$y(t) = y_{bl}(t) + y_{nl}(t), \tag{22}$$

*where $y_{bl}(t)$ is given in (15) and*

$$y_{nl}(t) = (\gamma - 1) \sum_{i=1}^{i=\mu-1} u_i(t_i^-) h_{ps}(t - t_i). \tag{23}$$

*Proof.* As previously demonstrated, at an arbitrary reset instant $t_i \in t_R$ $(i \in \mathbb{N})$, the control input signal of the RCS after the reset, $u(t_i^+)$, is equivalent to the base-linear signal $u_{bl}(t_i)$ augmented by a step signal of amplitude $(\gamma - 1)u(t_i^-)$. Consequently, the RCS in the time-domain can be viewed as its base-linear system and a discrete stair-step disturbance, denoted by $d_s(t)$, as defined below.

$$d_s(t) = (\gamma - 1) \sum_{i=1}^{i=\mu-1} u_i(t_i^-) h(t - t_i). \tag{24}$$

Thus, $y(t)$ is comprised of two elements: one is $y_{bl}(t)$ from the input $r(t)$; the other is $y_{nl}(t)$ in (23) from $d_s(t)$. □

Since MRCSs have multiple reset instances at discrete locations, the analysis of the corresponding disturbance signal $d_s(t)$ is complex. When the number of reset instants per period approaches infinity ($\mu \to \infty$), $\lim_{\mu\to\infty} d_s(t)$ is a continuous linear function when $t \in (t_1, \pi/\omega)$. In the following subsection, we analyse the boundary case of MRCSs, namely the Infinite-Reset Control Systems (IRCSs).

### *B. Frequency-domain Analysis of Infinite-reset Control Systems*

For the case of an IRCS, there are an infinite number of reset instants from $t_1$ until $t = \pi/\omega$ during the first half period.

**Theorem 2.** *(The frequency-domain based model for IRCSs) The output signal $y(t)$ and error signal $e(t)$ of a SISO IRCS with the input signal defined as $r(t) = R_0 \sin(\omega t)$ can be represented as*

$$\begin{aligned} y(t) &= y_{bl}(t) + \frac{\angle \mathcal{S}_{bl}(\omega)}{\pi} e_{bl}(t) + H_r(\omega, t),\\ e(t) &= (1 - \frac{\angle \mathcal{S}_{bl}(\omega)}{\pi}) \cdot e_{bl}(t) - H_r(\omega, t), \end{aligned} \tag{25}$$

*where $H_r(\omega, t)$ is given by*

$$\begin{aligned} H_r(\omega, t) =& |\mathcal{S}_{bl}(\omega)| \sum_{n=1}^{\infty} \frac{1}{n\pi} \sin(n\angle \mathcal{S}_{bl}(\omega)) \cdot [\sin((2n+1)\omega t + \\ & (n+1)\angle \mathcal{S}_{bl}(\omega)) - \sin((2n-1)\omega t + (n-1)\angle \mathcal{S}_{bl}(\omega))], \end{aligned} \tag{26}$$

*and $y_{bl}(t)$ and $e_{bl}(t)$ are given in (15).*

*Proof.* In IRCSs, during one period $(k\pi/\omega,\ (k+2)\pi/\omega),\ k \in \mathbb{N}$, the output $y(t)$ is given by

$$y(t) = \begin{cases} y_{bl}(t), & \text{for } t \in (k\pi/\omega,\ k\pi/\omega + t_1),\\ r(t), & \text{for } t \in (k\pi/\omega + t_1,\ (k+1)\pi/\omega). \end{cases} \tag{27}$$

In order to write the piece-wise affine function (27) to a Mixed Logical Dynamical (MLD) format, we introduce a square wave $s(t)$ as shown in Fig. 2 to separate the signals before and after $t_1$. $s(t)$ is given by

$$s(t) = \frac{\angle \mathcal{S}_{bl}(\omega)}{\pi} + \sum_{n=1}^{\infty} \frac{2}{n\pi} \sin(n\angle \mathcal{S}_{bl}(\omega)) \cos[2n\omega t + n\angle \mathcal{S}_{bl}(\omega)], \tag{28}$$

whose amplitudes alters between 0 and 1, period is $\frac{\pi}{\omega}$, and duty cycle is $\frac{\angle \mathcal{S}_{bl}}{\pi}$.
Thus, $y(t)$ in (27) and $e(t)$ can be derived as below:

$$\begin{aligned} &y(t) = y_{bl}(t) \cdot (1 - s(t)) + r(t) \cdot s(t) = y_{bl}(t) + e_{bl}(t) \cdot s(t),\\ &e(t) = r(t) - y(t) = (1 - s(t)) \cdot e_{bl}(t). \end{aligned} \tag{29}$$

Substitute (28) to (29), equation (25) is derived.

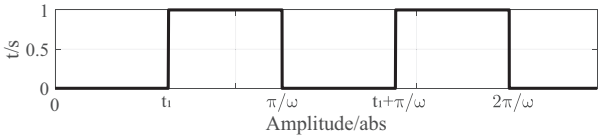


Fig. 2: Square wave $s(t)$ with amplitudes of 0 and 1.

Ignoring $d(t)$ and $n(t)$ in Fig. 1, based on (27), the new block diagram of the IRCS is shown in Fig. 3. □

Sensitivity functions of IRCSs are derived based on Theorem 2, as shown in the following Corollary.

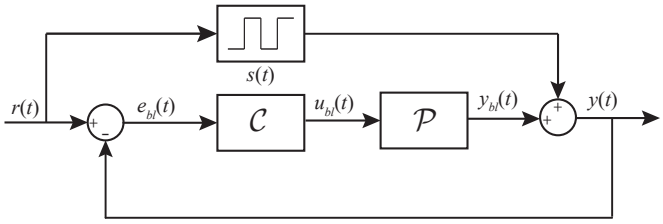


Fig. 3: The new block diagram of the IRCS.

**Corollary 1.** *(Sensitivity functions of IRCSs) In a SISO IRCS, the input signal is defined as* $r(t) = R_0 \sin(\omega t)$. *The n-th sensitivity function* $\overline{\mathcal{S}}_n(\omega)$, *complementary sensitivity function* $\overline{\mathcal{T}}_n(\omega)$, *and control sensitivity function* $\overline{\mathcal{CS}}_n(\omega)$ *of the IRCS are given in the following equations:*

$$\overline{\mathcal{S}}_n(\omega) = \begin{cases} \left(1 - \frac{\angle \mathcal{S}_{bl}(\omega)}{\pi}\right) \mathcal{S}_{bl}(\omega) - \frac{1}{\pi}|\mathcal{S}_{bl}(\omega)|\sin(\angle \mathcal{S}_{bl}(\omega)), & \text{for } n = 1, \\ -\frac{1}{k\pi}|\mathcal{S}_{bl}(\omega)|\sin(k\angle \mathcal{S}_{bl}(\omega))e^{j(k+1)\angle \mathcal{S}_{bl}(\omega)} - \\ \frac{1}{(k+1)\pi}|\mathcal{S}_{bl}(\omega)|\sin((k+1)\angle \mathcal{S}_{bl}(\omega))e^{jk\angle \mathcal{S}_{bl}(\omega)}, & \text{for odd } n = 2k+1, \\ 0, & \text{for even } n = 2k (k \in \mathbb{N}), \end{cases}$$

$$\overline{\mathcal{T}}_n(\omega) = \begin{cases} 1 - \overline{\mathcal{S}}_1(\omega), & \text{for } n = 1, \\ -\overline{\mathcal{S}}_n(\omega), & \text{for odd } n = 2k+1, \\ 0, & \text{for even } n = 2k (k \in \mathbb{N}), \end{cases}$$

$$\overline{\mathcal{CS}}_n(\omega) = \begin{cases} \overline{\mathcal{T}}_1(\omega)/\mathcal{P}(\omega), & \text{for } n = 1, \\ \overline{\mathcal{T}}_n(\omega)/\mathcal{P}(n\omega), & \text{for odd } n = 2k+1, \\ 0, & \text{for even } n = 2k (k \in \mathbb{N}). \end{cases} \tag{30}$$

### C. Comparison Metric

We define Prediction Error (PE) as follows:

$$\text{PE} = |\|y\|_{\text{Measured}} - \|y\|_{\text{Predicted}}|, \tag{31}$$

to describe the error between predicted results from the model and measured results from the simulation. Root mean square (RMS) ($L_2$ norm indicated as $\|.\|_2$) at steady-state are used as metrics to compare the difference between values. The PE of the new analysis method in Corollary 1 and the previous method in Proposition 2 (Two-reset Control System (2RCS) model) are defined as PE and PE′, respectively.

## IV. Results Discussion

We apply an RCS example $RCS_1$ to illustrate the effectiveness of the IRCS model. $RCS_1$ is comprised of a CI and a a Direct Current (DC) motor in [29]. Their base-linear transfer functions are

$$\mathcal{C}_{bl}(s) = \frac{1}{s} \text{ and } \mathcal{P}(s) = \frac{0.2}{0.1s^2 + 2.5s + 0.44}, \tag{32}$$

where the reset value is $\gamma = 0$.

Figure 4 (a) illustrates a comparison of the Phase Error (PE) of the $RCS_1$ based on the IRCS model (PE) and Two-reset Control System (2RCS) model (PE′). It can be observed that the PE of the IRCS model is less than that of the 2RCS model for frequencies below 0.037 Hz. Figure 4 (b) show the input signal $r(t)$ and error signal $e(t)$ when $f = 0.037$ Hz, which illustrates $f = 0.037$ Hz is closed to the critical frequency that separates the two-reset and multiple-reset scenarios in $RCS_1$. The results show than when there are more than two reset instants per period in an RCS, the new IRC model has better prediction performance than the 2RCS model.

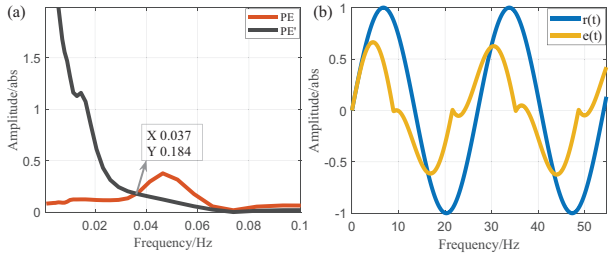


Fig. 4: (a) Prediction Error based on the IRCS (PE) and 2RCS (PE′) models, and (b) Time-domain response of $RCS_1$ when $f = 0.037$ Hz.

Figure 5 presents a comparison of the first-order sensitivity functions of the RCS in three scenarios: (1) assuming two resets per period utilising Proposition 2; (2) assuming infinite resets per period utilising Corollary 1; and (3) the Base-Linear System (BLS) without resets. The BLS is presented as a reference to demonstrate the differences between systems with and without resetting.

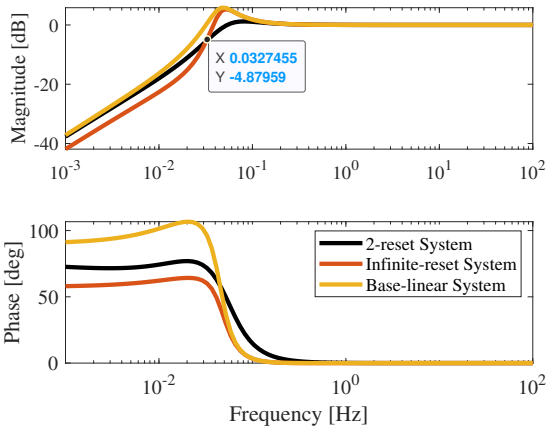


Fig. 5: Sensitivity function of the first order elements in "Two-reset system", "IRCS", "BLS".

The critical frequency (0.037 Hz) obtained through the PE analysis in Fig. 4 (a) corresponds to that (0.033 Hz) obtained through the sensitivity function analysis in Fig. 5. There is a slight deviation between these two critical points. Figure 6 visualises the first four harmonics of the sensitivity function in $RCS_1$ based on the IRCS model. We can see in the low frequencies, the higher order harmonics also contribute to the outputs of the system. The discrepancy between the two critical frequencies in Fig. 4 and 5 may be attributed to the fact that the sensitivity function in Fig. 5 only considers the first-order harmonic of the $RCS_1$ system.

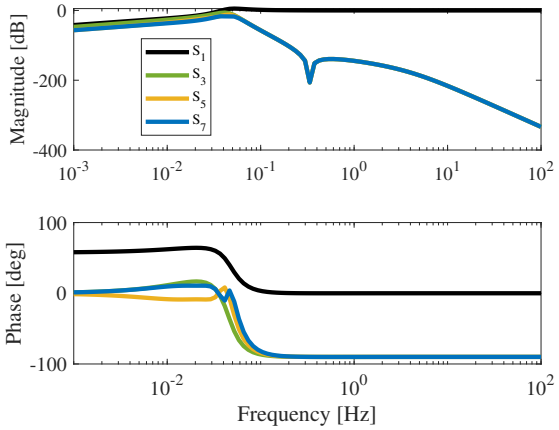


Fig. 6: The first four harmonics ($\mathcal{S}_1$, $\mathcal{S}_3$, $\mathcal{S}_5$, $\mathcal{S}_7$) of sensitivity function in the IRCS.

## V. Conclusion

The frequency-domain analysis technique of control systems is effective to quantify their performance in practice. Current frequency-domain analysis tools for RCSs are only valid when there are two resets per period. This study contributes to develop an analysis method for IRCSs in frequency domain, which serves as an extreme case of multiple-reset systems. The results show the proposed IRCS model demonstrates better prediction performance compared to the 2RCS model when the number of reset instants per period is high (much more than two). This method provides a foundation for the further analysis and design of MRCSs. Considerably more work regarding to the frequency-domain analysis of MRCSs will be done in the future.

## References


[1] Linda Chen, Niranjan Saikumar, Simone Baldi, and S Hassan HosseinNia. Beyond the waterbed effect: Development of fractional order crone control with non-linear reset. In *2018 annual american control conference (ACC)*, pages 545–552. IEEE, 2018.

[2] DA Deenen, Marcel François Heertjes, WPMH Heemels, and Henk Nijmeijer. Hybrid integrator design for enhanced tracking in motion control. In *2017 American Control Conference (ACC)*, pages 2863–2868. IEEE, 2017.

[3] Niranjan Saikumar, Kars Heinen, and S Hassan HosseinNia. Loop-shaping for reset control systems: A higher-order sinusoidal-input describing functions approach. *Control Engineering Practice*, 111:104808, 2021.

[4] John C Clegg. A nonlinear integrator for servomechanisms. *Transactions of the American Institute of Electrical Engineers, Part II: Applications and Industry*, 77(1):41–42, 1958.

[5] Isaac Horowitz and Patrick Rosenbaum. Non-linear design for cost of feedback reduction in systems with large parameter uncertainty. *International Journal of Control*, 21(6):977–1001, 1975.

[6] KR Krishnan and IM Horowitz. Synthesis of a non-linear feedback system with significant plant-ignorance for prescribed system tolerances. *International Journal of Control*, 19(4):689–706, 1974.

[7] Orhan Beker, CV Hollot, Yossi Chait, and Huaizhong Han. Fundamental properties of reset control systems. *Automatica*, 40(6):905–915, 2004.

[8] Alfonso Baños and Angel Vidal. Definition and tuning of a pi+ ci reset controller. In *2007 european control conference (ECC)*, pages 4792–4798. IEEE, 2007.

[9] Alfonso Baños, Sebastián Dormido, and Antonio Barreiro. Limit cycles analysis of reset control systems with reset band. *Nonlinear analysis: hybrid systems*, 5(2):163–173, 2011.

[10] Leroy Hazeleger, Marcel Heertjes, and Henk Nijmeijer. Second-order reset elements for stage control design. In *2016 American Control Conference (ACC)*, pages 2643–2648. IEEE, 2016.

[11] Niranjan Saikumar and Hassan HosseinNia. Generalized fractional order reset element (gfrore). In *9th European Nonlinear Dynamics Conference (ENOC)*, 2017.

[12] Christoph Weise, Kai Wulff, and Johann Reger. Fractional-order memory reset control for integer-order lti systems. In *2019 IEEE 58th conference on decision and control (CDC)*, pages 5710–5715. IEEE, 2019.

[13] Niranjan Saikumar, Rahul Kumar Sinha, and S Hassan HosseinNia. "constant in gain lead in phase" element–application in precision motion control. *IEEE/ASME Transactions on Mechatronics*, 24(3):1176–1185, 2019.

[14] SJLM Van Loon, KGJ Gruntjens, Marcel François Heertjes, Nathan van de Wouw, and WPMH Heemels. Frequency-domain tools for stability analysis of reset control systems. *Automatica*, 82:101–108, 2017.

[15] PWJM Nuij, OH Bosgra, and Maarten Steinbuch. Higher-order sinusoidal input describing functions for the analysis of non-linear systems with harmonic responses. *Mechanical Systems and Signal Processing*, 20(8):1883–1904, 2006.

[16] Pieter Nuij, Maarten Steinbuch, and Okko Bosgra. Measuring the higher order sinusoidal input describing functions of a non-linear plant operating in feedback. *Control Engineering Practice*, 16(1):101–113, 2008.

[17] Levent Ucun and Jan Salášek. Hosidf-based feedforward friction compensation in low-velocity motion control systems. *Mechatronics*, 24(2):118–127, 2014.

[18] Ali Ahmadi Dastjerdi, A Astolfi, Niranjan Saikumar, N Karbasizadeh, Duarte Valerio, and S Hassan HosseinNia. Closed-loop frequency analysis of reset control systems. *arXiv preprint arXiv:2001.10487*, 2020.

[19] Xinxin Zhang, Marcin B Kaczmarek, and S Hassan HosseinNia. Frequency-domain analysis for reset systems using pulse-based model. *arXiv preprint arXiv:2206.00523*, 2022.

[20] José Antonio González Prieto, Antonio Barreiro, and Sebastián Dormido. Frequency domain properties of reset systems with multiple reset anticipations. *IET Control Theory & Applications*, 7(6):796–809, 2013.

[21] Nima Karbasizadeh, Ali Ahmadi Dastjerdi, Niranjan Saikumar, and S Hassan HosseinNia. Band-passing nonlinearity in reset elements. *arXiv preprint arXiv:2009.06091*, 2020.

[22] Alfonso Banos and Antonio Barreiro. *Reset control systems*. Springer, 2012.

[23] Yuqian Guo and Yanying Chen. Stability analysis of delayed reset systems with distributed state resetting. *Nonlinear Analysis: Hybrid Systems*, 31:265–274, 2019.

[24] Yuqian Guo, Lihua Xie, and Youyi Wang. *Analysis and Design of Reset Control Systems*. 11 2015.

[25] Dragan Nešić, Luca Zaccarian, and Andrew R Teel. Stability properties of reset systems. *Automatica*, 44(8):2019–2026, 2008.

[26] Ali Ahmadi Dastjerdi, Alessandro Astolfi, and S Hassan HosseinNia. A frequency-domain stability method for reset systems. In *2020 59th IEEE Conference on Decision and Control (CDC)*, pages 5785–5791. IEEE, 2020.

[27] CV Hollot, Orhan Beker, Yossi Chait, and Qian Chen. On establishing classic performance measures for reset control systems. In *Perspectives in robust control*, pages 123–147. Springer, 2001.

[28] Kars Heinen. Frequency analysis of reset systems containing a clegg integrator: An introduction to higher order sinusoidal input describing functions. 2018.

[29] PM Meshram and Rohit G Kanojiya. Tuning of pid controller using ziegler-nichols method for speed control of dc motor. In *IEEE-international conference on advances in engineering, science and management (ICAESM-2012)*, pages 117–122. IEEE, 2012.